Supporting Information

Cr-doped Pd metallene nanoribbon superstructures for oxygen reduction reaction and formic acid oxidation

Shanshan Chen[a], Qiang Yuan[a*] and Xun Wang[b*]

Experimental Section

Materials

Ammonium tetrachloropalladate ($(NH_4)_2PdCl_4$, 97%), chromium hexacarbonyl ($Cr(CO)_6$, 99%), Hexadecyl trimethyl ammonium bromide (CTAB, 99%), polyvinylpyrrolidone (PVP-8000), Absolute methanol, HCOOH and N,N-dimethylformamide (DMF, 99.8) were purchased from Aladdin. Formaldehyde (HCHO, 37%) were obtained from Alfa Aesar. KOH (AR) and Chromium (III) acetylacetonate($Cr(acac)_3$, 98%) were purchased from Macklin. Pt/C (20 wt %, 60 wt %) and Pd/C (20 wt %) was obtained from Johnson Matthey. Vulcan XC-72 was got from Cabot.

Synthesis of 3D PdCr MNR catalysts

In a typical synthesis, 8.6 mg of $(NH_4)_2PdCl_4$, 4.4 mg of $Cr(CO)_6$, 40 mg of CTAB, 100 mg PVP, 0.1 mL of formaldehyde and 10 mL DMF were added to a 20 mL Teflon-lined stainless-steel autoclave, followed by stirring for 15 minutes. The mixture was transferred to an oven and heated at 150 °C for 12 h. The synthesized product was cooled to room temperature, centrifuged with ethanol and washed three times (10,000 rpm for 15 min). Finally, the obtained 3D PdCr MNR was preserved in ethanol.

Characterizations

The shape and size of samples were analysed by Transmission electron microscope (TEM; JEM-1400 Flash at 120KV) and double spherical aberration-corrected (AC) transmission electron microscopy high-resolution (FEI, Themis Z). The inductively coupled plasma optical emission spectrometry (ICP-OES) (Thermo Fisher Scientific, iCAP 7200) was used to analyze composition of samples. The X-ray diffraction (XRD)

patterns of the samples were recorded on a Bruker D8 Advance diffractometer with Cu Kα radiation (λ=1.5418 Å) with graphite monochromator (40 KV, 40 mA). X-ray photoelectron spectroscopy (XPS) measurements were performed using AlK_a X-ray radiation (1486.6 eV) for excitation at 150 W (Thermo Fisher Scientific, USA).

Measurement of ORR

Electrochemical tests were carried out on CHI760E electrochemical analyzer (CHI instrument, Shanghai, ChenHua Co., Ltd.) using a three-electrode system. Glassy carbon (GC, Φ = 5 mm, 0.196 cm^2) rotating disk electrode (RDE) (PINE, USA) was used as the working electrode, while Hg/HgO electrode and graphite rod were the reference and counter electrodes, respectively. 200 μL of the 3D PdCr MNR catalyst, 1 mg of XC-72 and 50 μL Nafion (1 wt %) were dispersed in 750 μL isopropanol. The ink was formed after 45 minutes ultrasound. All the electrochemical measurements were conducted at room temperature. The suspension of catalysts was spread on the GC electrode, and the Pd/Pt loading on GC was in the range of 10~10.7 ug cm^{-2}. The cyclic voltammetry (CV) curves were recorded in N_2-saturated 0.1 M KOH solution at a sweep rate of 50 mV s^{-1}. The ORR measurements were performed in O_2-saturated 0.1 M KOH solutions at a scan rate of 10 mV s^{-1} and a rotation speed of 1600 rpm. The LSV polarization curve of ORR was normalized with geometric area unless otherwise marked.

DMFC test

At the anode, catalyst inks were made by mixing Pt/C (60 wt.%), 200 μL water, 3 mL isopropanol, and 100 μL polytetrafluoroethylene (PTFE) solution (15 wt %). The anode catalyst was coated with nickel foam (2×2 cm^2). At the cathode, Pt/C (60 wt %) or 3D PdCr MNR/XC-72 mixtures were dispersed in 200 μL water, 3mL isopropanol and 100 μL Nafion solution (5 wt %), and the ensuing mixture was subjected to ultrasound for 45 min. The cathode catalyst was coated on a gas diffusion layer (2×2 cm^2). The metal (Pt) loading of both the anode and cathode catalysts were 0.8 mg cm^{-2}. Anion exchange membrane (FAAM-20) was immersed in 6 M

potassium hydroxide solution at 60°C for 24 h, followed by polarization curve measurements using a fuel cell test system (850e, Scribner Associates Inc.). The anode fuel was 6 M KOH + 6 M CH_3OH solution with an injection rate of 2 mL min^{-1}, the cathode gas was O_2, and the flow rate was 200 mL min^{-1}. The performance of the battery was carried out at 80°C.

The computing method of ECSA

In alkaline solution, the electrochemically active surface area (ECSA) can be calculated from charges changes in the reduction region of PdO according to the equation as follow:

$$ECSA = Q/(0.405 \times Pd_m)$$

Pd_m is associated with the loading of Pd on the work electrode, 0.405 mC cm^{-2} is a constant assuming that a monolayer of PdO was reduced on the Pd surface and Q (mC) is the reduction charge of PdO.

The ECSA of Pt/C were calculated by the following equation:

$$ECSA = Q_H/(210 \times Pt_m),$$

Q_H is the charge for Hupd adsorption determined using $Q_H = 0.5 \times Q$, Pt_m is associated with the loading of Pt on the work electrode, and 210 μC cm^{-2} is the charge required for the monolayer adsorption of hydrogen on the Pt surface.

Accelerated durability tests

The accelerated durability tests were carried out in O_2-saturated 0.1 M KOH solution by applying cyclic potential sweeps between 0.57 and 1.07 V (at 0.9 V vs. RHE) at a sweep rate of 100 mV s^{-1}.

Methanol tolerance test

The measurements of methanol tolerance were performed by directly introducing 0.1 M CH_3OH into electrolyte solution during ORR test.

In situ anti-CO performance

In situ anti-CO experiments for ORR were tested in 0.1 M KOH solution at a scan rate of 10 mV s^{-1} and a rotation speed of 1600 rpm. After obtaining a stable polarization curve in O_2-saturated solution, CO gas was introduced at a flow rate of

10 mL min^{-1} for 5 minutes, and the CO gas stream was maintained during the polarization curve measurement.

The electron transfer number (n) and the peroxide yield (H_2O_2%)

The electron transfer number and the corresponding H_2O_2 formation of the ORR can be estimated according to the following equations:

$$\frac{4I_d}{I_d + I_r/N}$$

$$H_2O_2\% = \frac{200I_r/N}{I_d + I_r/N}$$

where I_d and I_r are the disk and ring current measured from the RRDE tests and N (0.37) represents the collection efficiency of the Pt ring.

Formic acid oxidation (FAO) performance

The cyclic voltammetry (CV) curves were recorded in the N_2-saturated 0.1 M $HClO_4$ solution or 0.1 M $HClO_4$ + 0.5 M HCOOH solution, a Ag/AgCl electrode and a graphite rod were used as the reference and counter electrode, respectively. The suspension of catalysts was spread on the GC electrode. And the potential was scanned from -0.25 to 0.9 V (Ag/AgCl) at a scan rate of 50 mV s^{-1}. Later, the current–time (i-t) test was performed at 0.1 V for 3600 s.

DFAFC test

Pt/C (60 wt %) or 3D PdCr MNR/XC-72 mixtures were dispersed in 100 μL water, 1mL isopropanol and 30 μL Nafion solution (5 wt %), The cathode catalyst Pt/C and the anode catalyst 3D PdCr MNR/C were coated on a gas diffusion layer (2×2 cm^2), respectively. The metal (Pt) loading of both the anode and cathode catalysts were 0.4 mg cm^{-2}. The Nafion115 membranes were treated with hydrogen peroxide, sulfuric acid, and water at 80°C for 30 min respectively. Followed by polarization curve measurements using a fuel cell test system (850e, Scribner Associates Inc.). The anode fuel was 3 M HCOOH solution with an injection rate of 3 mL min^{-1}, the cathode gas was O_2, and the flow rate was 300 mL min^{-1}. The performance of the battery was carried out at 80 °C.

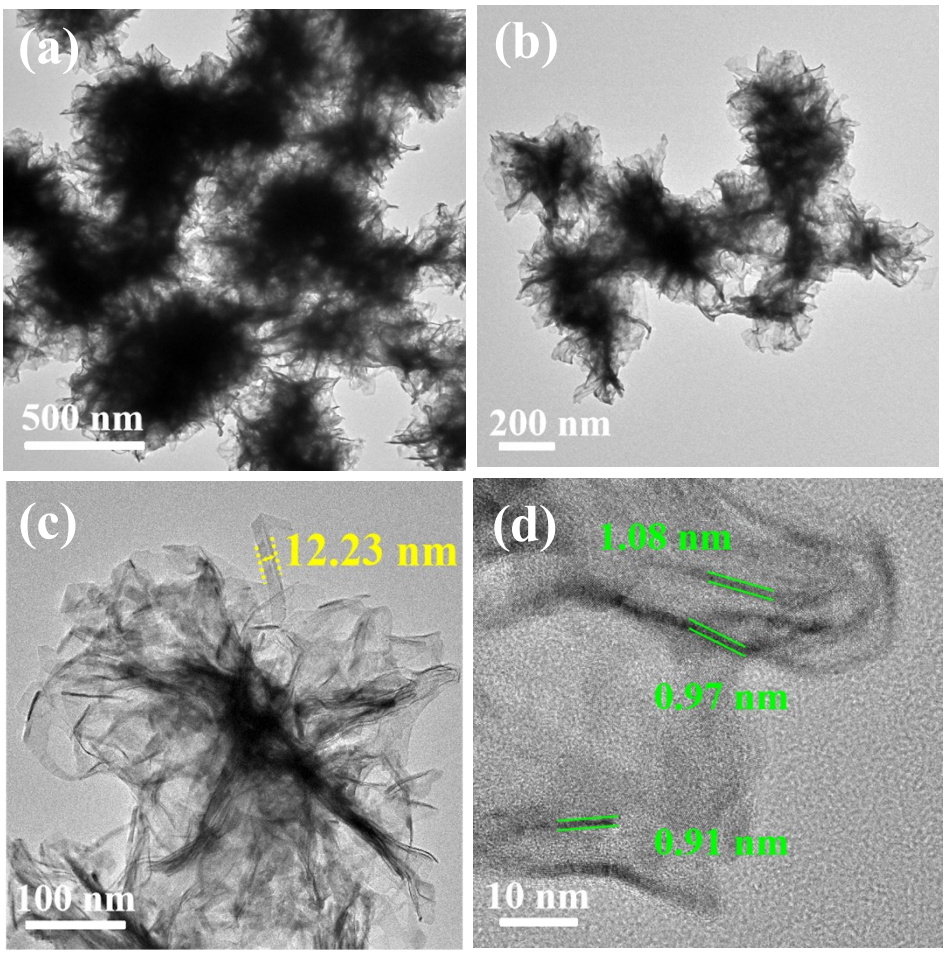

Fig. S1 (a-c) TEM and (d) spherical AC-HRTEM images of 3D PdCr MNR.

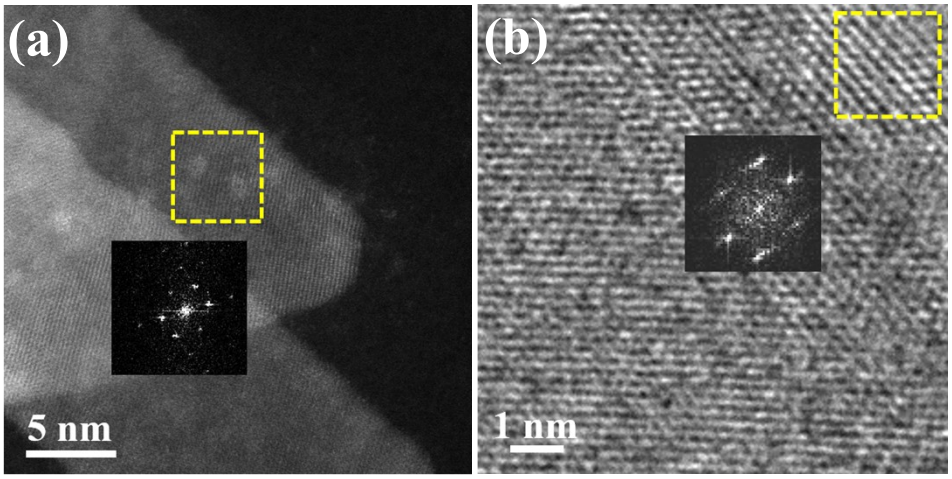

Fig. S2 (a,b) Spherical AC-HRTEM images and the corresponding FFT patterns of

3D PdCr MNR obtained in different regions.

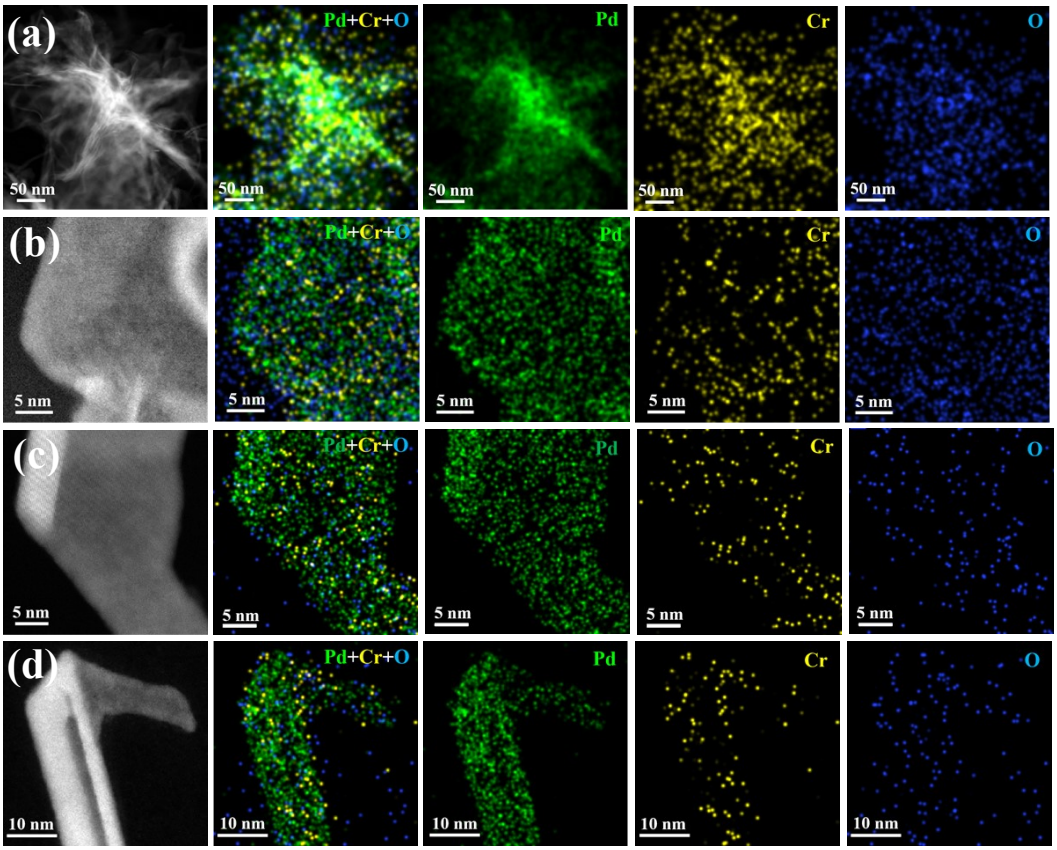

Fig. S3 (a)-(d) Spherical AC HAADF-STEM images and corresponding elemental mappings of 3D PdCr MNR at different positions and magnifications. (Pd: green, Cr: yellow and O: blue)

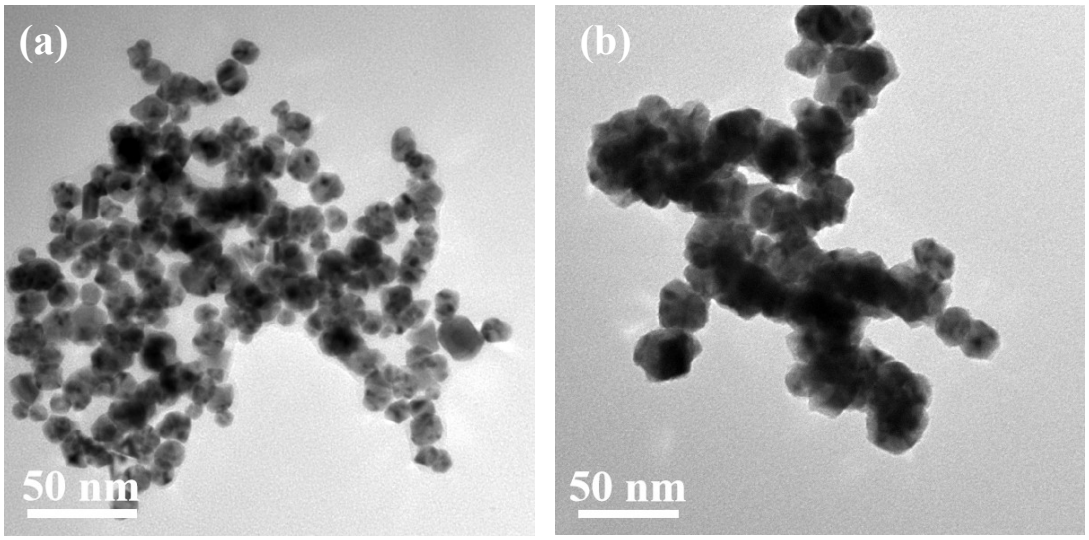

Fig. S4 TEM images of products collected from the reaction with the same conditions used in the synthesis of 3D PdCr MNR. (a) in the absence of $Cr(CO)_6$. (b) Use $Cr(acac)_3$ instead of $Cr(CO)_6$.

Table S1. XRD informations of different samples.

Sample	2θ	d (Å)	a (Å)	Strain (%)
Pd (PDF-46-1043)	40.119	2.248	3.893	/
3D PdCr MNR	39.642	2.273	3.937	1.13

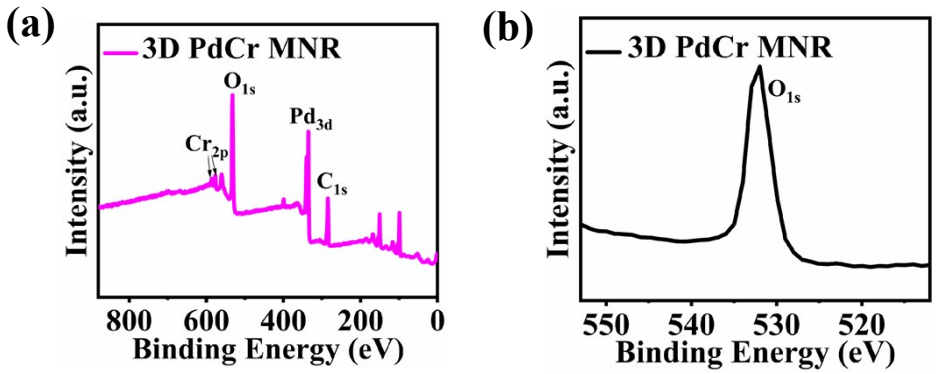

Fig. S5 (a) XPS full spectra, (b)XPS spectra of O_{1s} for 3D PdCr MNR.

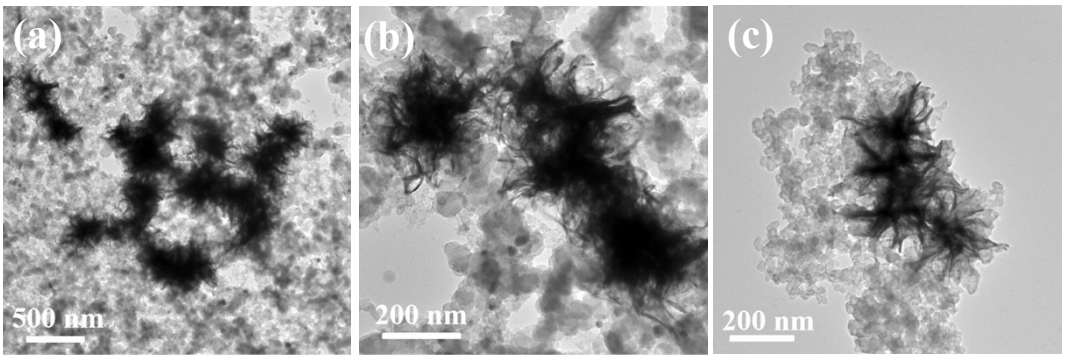

Fig. S6 (a-c) TEM images of 3D PdCr MNR/C.

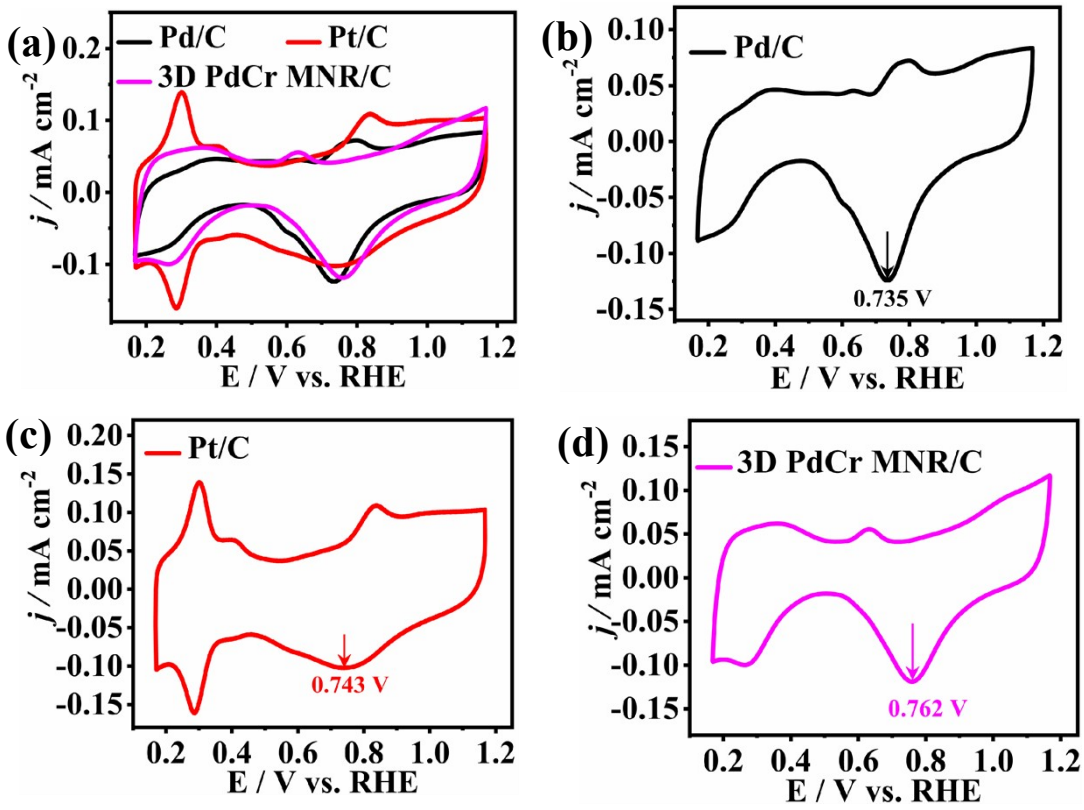

Fig. S7 Cyclic voltammetry (CV) curves of commercial Pd/C, Pt/C and 3D PdCr MNR/C in 0.1 M KOH solution.

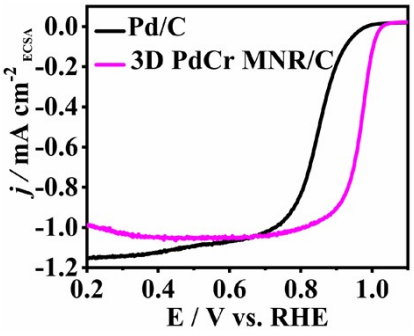

Fig. S8 ECSA-normalized LSV curves of commercial Pd/C and 3D PdCr MNR/C in 0.1 M KOH before stability.

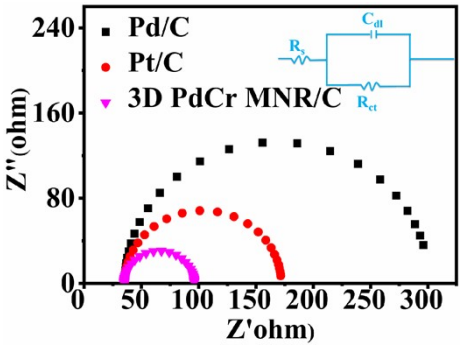

Fig. S9 Electrochemical impedance spectroscopy (EIS) of the as-synthesized Pd/C, Pt/C and 3D PdCr MNR/C. EIS was carried out in O_2-saturated 0.1 mol L^{-1} KOH at 0.9 V (vs. RHE), in the frequency range from 100 kHz to 0.01 Hz with a rotation rate of 1600 rpm (inset is the equivalent circuit).

The EIS test is a standard three-electrode system with multiple contact interfaces. Between the working electrode and the reference electrode is the range of the applied AC frequency (sine wave) potential signal. Within this interval, the following components can be considered: 1) the resistance of the cable; 2) the resistance inside the working electrode; 3) the resistance of the contact interface between the working electrode and the solution; 4) the resistance of the solution between the working electrode and the reference electrode; 5) the capacitance caused by the double electric layer at the contact interface between the working electrode and the solution. Among them, since the cable resistance, the resistance inside the working electrode, and the solution resistance between the working electrode and the reference electrode are all in a series state, they can be considered as one resistance according to the physical theory. The resistance of the contact interface and the capacitance caused by the contact interface double layer are considered to be in parallel because they are generated at the same location.

Therefore, the following equivalent circuit diagram is also formed.

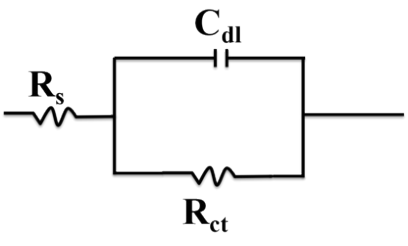

Where R_S is the resistance of the electrolyte, C_{dl} is the double layer capacitance of the working electrode and Rct is the resistance of the electron transfer by the redox reaction in the double layer.

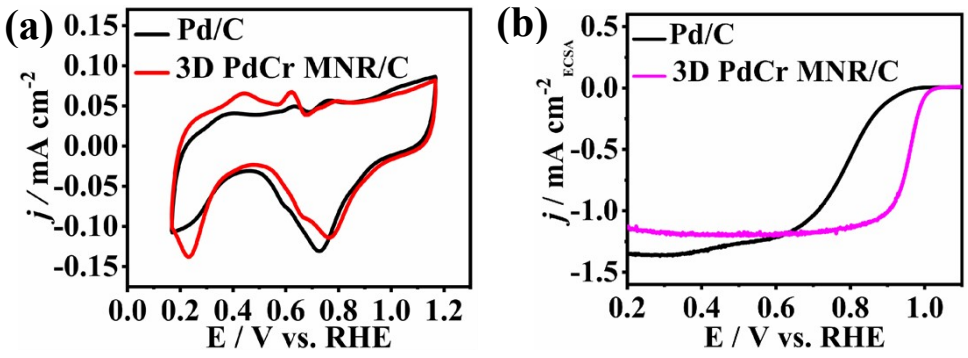

Fig. S10 (a) CV curves and (b) ECSA-normalized LSV curves of commercial Pd/C and 3D PdCr MNR/C in 0.1 M KOH after stability.

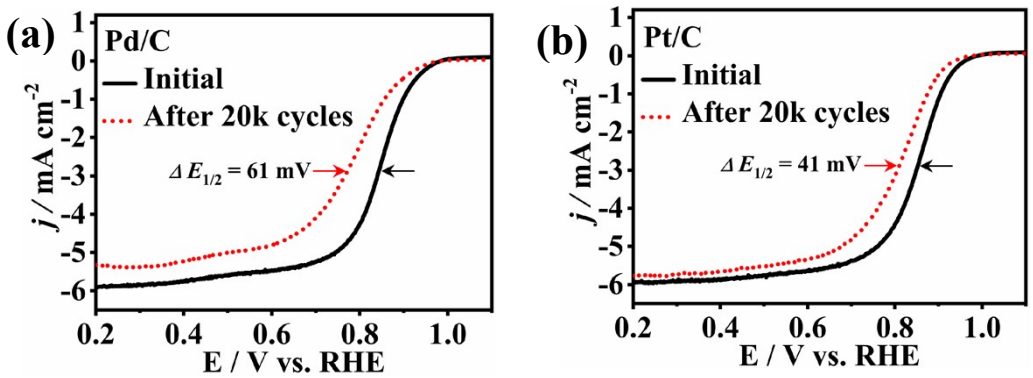

Fig. S11 ORR polarization curves of commercial (a) Pd/C and (b) Pt/C in 0.1 M KOH solution obtained after scanning 20,000 cycles.

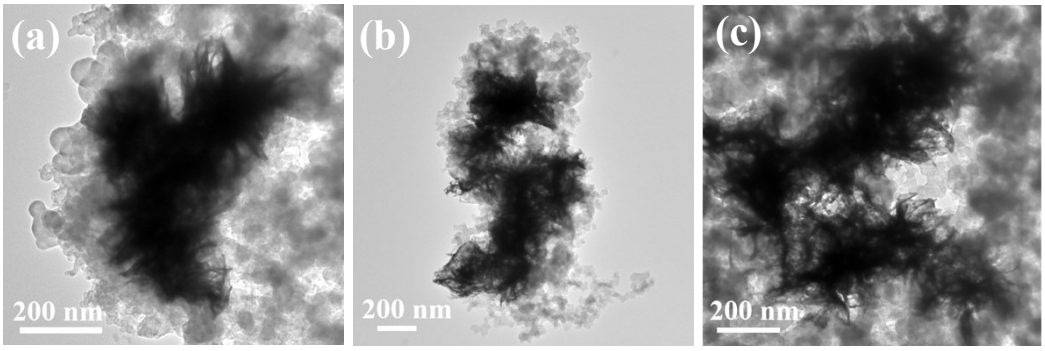

Fig. S12 (a-c) TEM images of after scanning 20,000 cycles for 3D PdCr MNR/C.

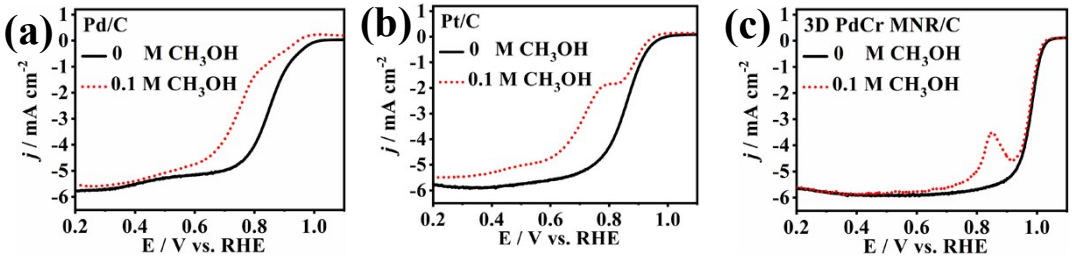

Fig. S13 ORR polarization curves of (a) commercial Pd/C, (b) Pt/C and (c) 3D PdCr MNR/C in 0.1 M KOH + 0.1 CH_3OH alkaline solution.

Table S2. Comparison of mass activity with reported Pd-based catalysts towards the ORR in alkaline medium.

Catalysts	Half Wave Potential ($E_{1/2}$)(V)	Mass Activity (A/mg)	Specific Activity (mA/cm^2)	Reference
3D PdCr MNR	0.968	3.29	5.56	This work
c-Pd metallene	0.947	2.76	8.14	[1]Adv. Mater. 2022, 34, 2202084.
Pd@PANI metallene	0.97	1.79	2.96	[2]Appl. Catal. B: Environ. 2015, 307, 35−42.
Pd metallene /C	0.9	0.892	1.336	[3]Angew. Chem. Int. Ed. 2021, 60, 12027−12031.
Fe−Pd UPM	0.914	0.736	0.225	[4]ACS Nano 2022, 16, 522−532.
RuOx-on-Pd NSs/C	0.93	1.52	1.87	[5]Angew. Chem. Int. Ed. 2021, 60, 16093−16100.
Pd_3Pb UPINs	0.908	0.59	1.18	[6]Angew. Chem. Int. Ed. 2021, 60, 10942−10949.
$Pd_9Pt_1Ni_1$ NSs	0.928	0.29	1.22	[7]Small 2022, 18, 2103665.
WPd-H NSAs	/	1.51	2.56	[8]Energy Fuels 2022, 36, 7775−7781.
Pd_{NS}/WNi/C	0.906	0.496	/	[9]ACS Catal. 2020, 10, 4290−4298.

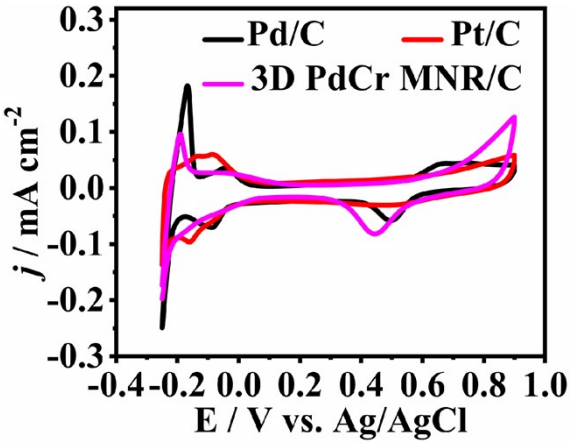

Fig. S14 Cyclic voltammetry (CV) curves of commercial Pd/C, Pt/C and 3D PdCr MNR in 0.1 M $HClO_4$ solution.

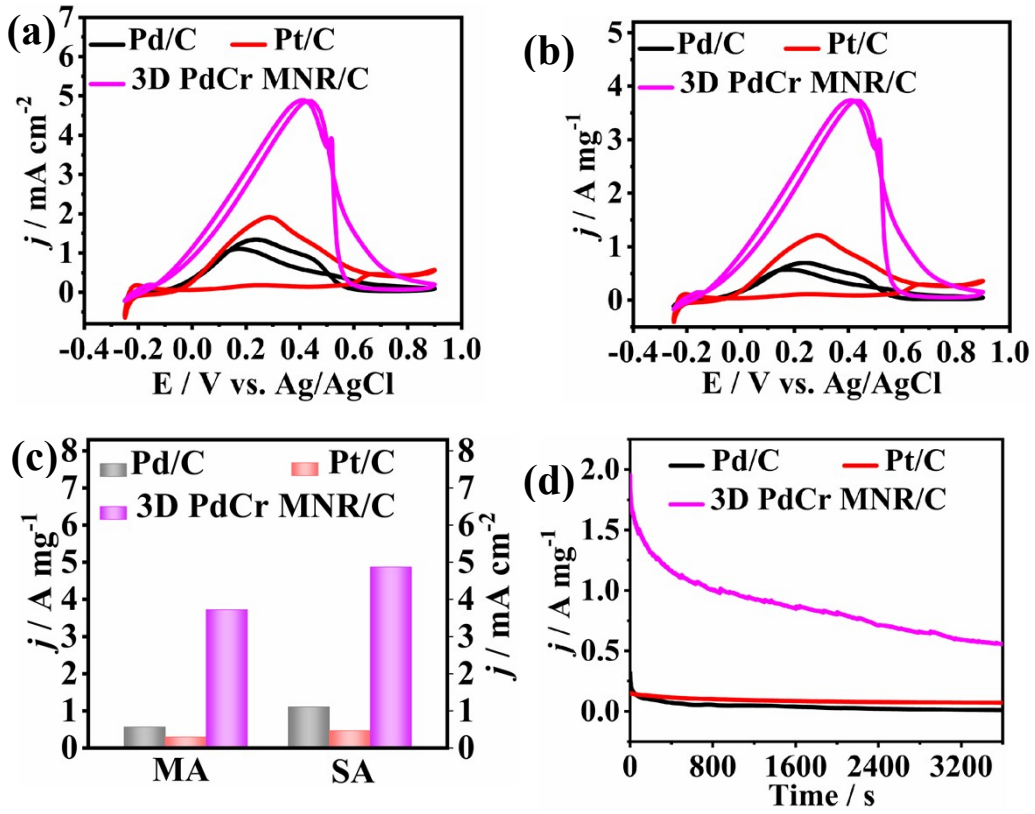

Fig. S15 Cyclic voltammetry (CV) curves (specific activity (a) and mass activity (b)) of 3D PdCr MNR/C, commercial Pt/C and Pd/C in 0.1 M $HClO_4$+ 0.5 M HCOOH solution. (c) MA and SA

histograms of 3D PdCr MNR/C, commercial Pd/C and Pt/C. (d) Current–time curves of 3D PdCr MNR, commercial Pt/C, and Pd/C in 0.1 M $HClO_4$ + 0.5 M HCOOH solution.

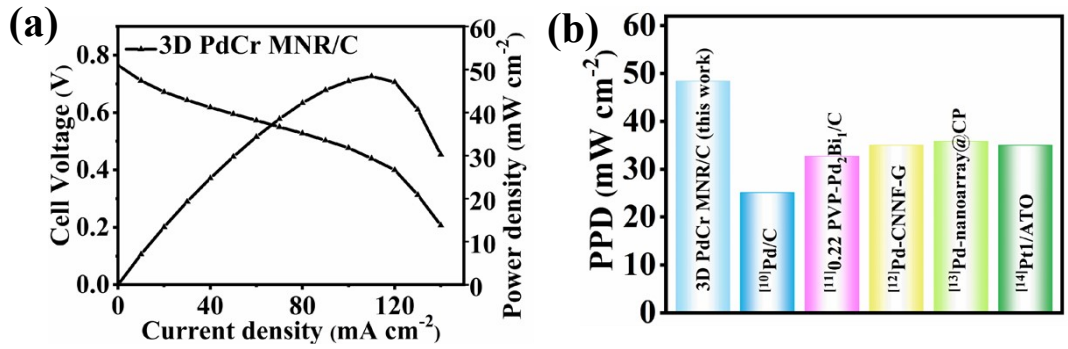

Fig. S16 (a) Power density and polarization curves of the direct formic acid fuel cell of 3D PdCr MNR/C. (b) Comparison of the peak power density (PPD) of 3D PdCr MNR/C with published catalysts in direct formic acid fuel cells (Reference 10-14).

References

1 F. X. Lin, F. Lv, Q. H. Zhang, H. Luo, K. Wang, J. H. Zhou, W. Y. Zhang, W. S. Zhang, D. W. Wang, L. Gu and S. J. Guo, Local Coordination Regulation through Tuning Atomic-Scale Cavities of Pd Metallene toward Efficient Oxygen Reduction Electrocatalysis, *Adv. Mater.,* 2022, **34**, 2202084.

2 H. J. Wang, W. X. Wang, H. J. Yu, Q. Q. Mao, Y. Xu, X. N. Li, Z. Q. Wang, L. Wang, Interface Engineering of Polyaniline-Functionalized Porous Pd Metallene for Alkaline Oxygen Reduction Reaction, *Appl. Catal. B: Environ.,* 2015, **307**, 121172.

3 H. J. Yu, T. Q. Zhou, Z. Q. Wang, Y. Xu, X. N. Li, L. Wang and H. J. Wang, Defect-Rich Porous Palladium Metallene for Enhanced Alkaline Oxygen Reduction Electrocatalysis, *Angew. Chem. Int. Ed.,* 2021, **60**, 12027−12031.

4 S. D. Huang, S. L. Lu, S. Gong, Q. J. Zhang, F. Duan, H. Zhu, H. W. Gu, W. F. Dong and M. L. Du, Sublayer Stable Fe Dopant in Porous Pd Metallene Boosts Oxygen Reduction Reaction, *ACS Nano,* 2022, **16**, 522−532.

5 Z. X. Lyu, X.G. Zhang, Y. C. Wang, K. Liu, C. Y. Qiu, X. Y. Liao, W. H. Yang, Z. X. Xie, and

S. F. Xie, Amplified Interfacial Effect in an Atomically Dispersed RuOx-on-Pd 2D Inverse Nanocatalyst for High-Performance Oxygen Reduction, *Angew. Chem. Int. Ed.,* 2021, **60**, 16093–16100.

6 J. C. Guo, L. Gao, X. Tan, Y. L. Yuan, J. Kim, Y. Wang, H. Wang, Y. J. Zeng, S. Choi, S. C. Smith and H. W. Huang, Template-Directed Rapid Synthesis of Pd-Based Ultrathin Porous Intermetallic Nanosheets for Efficient Oxygen Reduction, *Angew. Chem. Int. Ed.,* 2021, **60**, 10942−10949.

7 L. J. Shi, Q. Wang, Q. Ren, Q. Yang, D. H. Zhao, Y. H. Feng, H. Y. Chen and Y. W. Wang, Facile Synthesis of Pd and PdPtNi Trimetallic Nanosheets as Enhanced Oxygen Reduction Electrocatalysts, *Small,* 2022, **18**, 2103665.

8 H. J. Wang, T. Q. Zhou, K. Deng, W. J. Tian, H. J. Yu, Y. Xu, X. N. Li, Z.Q. Wang, and L. Wang, Ultrathin Porous WPdH Nanosheet Assemblies for Efficient Alkaline Oxygen Reduction, *Energy Fuels,* 2022, **36**, 7775−7781.

9 L. Song, Z. X. Liang, K. Nagamori, H. Igarashi, M. B. Vukmirovic, R. R. Adzic and K. Sasaki, Enhancing Oxygen Reduction Performance of Pt Monolayer Catalysts by Pd(111) Nanosheets on WNi Substrates, *ACS Catal.,* 2020, **10**, 4290−4298.

10 P. Hong, F. Luo, S. J. Liao and J. H. Zeng, Effects of Pt/C, Pd/C and PdPt/C Anode Catalysts on the Performance and Stability of Air Breathing Direct Formic Acid Fuel Cells, *Int. J. Hydrog. Energy*, 2011, **36**, 8518–8524.

11 S. W. Yang, J. W. Yang, Y. J. Chung and Y. C. Kwon, Pd−Bi Bimetallic Catalysts Including Polyvinylpyrrolidone Surfactant Inducing Excellent Formic Acid Oxidation Reaction and Direct Formic Acid Fuel Cell Performance, *Energy,* 2017, **36**, 17211−17220.

12 W. Y. Zhang, Q. S. Yao, X. D. Wu, Y. s. Fu, K. M. Deng and X. Wang, Intimately Coupled Hybrid of Graphitic Carbon Nitride Nanoflakelets with Reduced Graphene Oxide for Supporting Pd Nanoparticles: A Stable Nanocatalyst with High Catalytic Activity Towards Formic Acid and Methanol Electrooxidation, *Electrochim. Acta.,* 2016, **200**, 131−141.

13 Y. Zhou, Y. Yang, X. Zhu, T. Zhang, D. D. Ye, R. Chen and Q. Liao, Novel Superaerophobic Anode with Fern-Shaped Pd Nanoarray for High-Performance Direct Formic Acid Fuel Cell, *Adv. Funct. Mater.,* 2022, **32**, 2201872.

14 J. Kim, C. W. Roh, S. K. Sahoo, S. Yang, J. Bae, J. W. Han and H. Lee, Highly Durable

Platinum Single-Atom Alloy Catalyst for Electrochemical Reactions, *Adv. Energy Mater.,* 2017, **8**, 1701476.